THE JOURNAL OF PHYSICAL CHEMISTRY C

Article

pubs.acs.org/JPCC

Singlet Oxygen Generation by Laser Irradiation of Gold Nanoparticles

Samantha J. Chadwick,[†] Dina Salah,[†,§] Penelope M. Livesey,[†] Mathias Brust,[†] and Martin Volk*[,‡]

[†]Department of Chemistry, University of Liverpool, Crown Street, Liverpool L69 7ZD, United Kingdom

[‡]Surface Science Research Centre, Department of Chemistry, University of Liverpool, Abercromby Square, Liverpool L69 3BX, United Kingdom

[§]Biophysics Group, Physics Department, Ain Shams University, Cairo, Egypt

Supporting Information

ABSTRACT: The formation of singlet oxygen by irradiation of gold nanoparticles in their plasmon resonance band with continuous or pulsed laser light has been investigated. Citrate-stabilized nanoparticles were found to facilitate the photogeneration of singlet oxygen, albeit with low quantum yield. The reaction caused by pulsed laser irradiation makes use of the equilibrated hot electrons that can reach temperatures of several thousand degrees during the laser pulse. Although less efficient, continuous irradiation, which acts via the short-lived directly excited primary "hot" electrons only, can produce enough singlet oxygen for photodynamic cancer therapy and has significant advantages for practical applications. However, careful design of the nanoparticles is needed, since even a moderately thick capping layer can completely inhibit singlet oxygen formation. Moreover, the efficiency of the process also depends on the nanoparticle size.

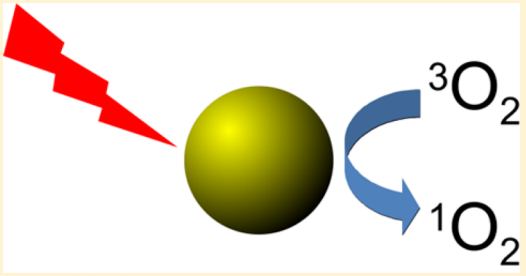

INTRODUCTION

In recent years, nanoparticles have been used increasingly for biomedical applications, including drug or gene delivery, imaging, sensing, or photothermal therapy.[1−6] In particular, gold nanoparticles (NPs) have been suggested as highly useful sensitizing agents in phototherapy due to their unique size and shape-dependent optical properties, high absorption coefficients, ease of synthesis, biocompatibility, and their ability to hold a variety of functional ligands.[5−7] It is well-known that citrate-stabilized gold NPs are endocytosed by cells and remain in intracellular vesicles.[8] Moreover, targeting of specific sites inside the cell by functionalization of the surface with cell penetrating peptides or peptides containing nuclear localization sequences has been reported.[9] Alternatively, to selectively target specific types of cells, gold NPs can be modified with suitable antibodies. This approach has been studied for potential use in photothermal cancer therapy, where cancer cells overexpressing human epidermal growth factor receptor 2 (HER2) or epithelial growth factor receptor (EGFR) were incubated with gold NPs conjugated to anti-HER2[10] or anti-EGFR[11−13] antibodies, respectively. The NPs were then irradiated with light within their plasmon resonance absorbance band to heat the cells to temperatures leading to cell death.[13−15]

Most interestingly, it has also been demonstrated that endocytosis of gold NPs by cancer cells and subsequent irradiation of such intracellular NPs can lead to cell death even at irradiation levels that are not high enough to cause significant heating.[16−18] This nonthermal route to laser-induced cell death has been ascribed to an as yet not fully characterized photochemical reaction, although irradiation of endocytosed NPs was reported to be accompanied by increased levels of reactive oxygen species.[16,17] The use of such a photochemical mechanism could be of great advantage in situations where different types of cells coexist in close vicinity, since it would allow for more selective targeting of particular cells, whereas—due to the fast diffusion of heat over the relevant length scales—photothermally induced cell death will affect all cells within the irradiated volume more or less indiscriminately, as long as some of them contain NPs.

Irradiation of gold NPs with continuous wave (CW) lamp or laser light has been shown to lead to photogeneration of singlet oxygen ($^1O_2$) *in vitro*,[17−21] suggesting that this highly reactive species, which is widely used in photodynamic therapy,[22,23] may be involved in the photochemical pathway of cell killing by gold NPs. *In vitro* $^1O_2$ photogeneration by irradiation of spherical gold NPs with short laser pulses *or* CW laser light at comparable powers and intensities has also been reported.[24] In this study, it was suggested that the mechanism of singlet oxygen photogeneration may involve "hot" electrons, i.e., the highly excited conduction band electrons which upon absorption of a short laser pulse by a NP can reach quasi-equilibrated energy distributions corresponding to temperatures of several thousand degrees.[25,26] This seems somewhat surprising, since CW light at the intensities used does not yield "hot" electrons due to the rapid electronic relaxation occurring in gold NPs.[25−27]

Received: February 26, 2016
Revised: May 3, 2016
Published: May 5, 2016

DOI: 10.1021/acs.jpcc.6b02005
J. Phys. Chem. C 2016, 120, 10647−10657

Here we present new experimental results on the photogeneration of singlet oxygen by irradiation of gold nanoparticles with continuous *or* pulsed laser light, as well as theoretical work pertaining to the underlying mechanism(s), which so far had not been addressed. We show that electron temperatures in excess of 2000 °C are easily achieved in pulsed laser irradiation experiments, whereas CW light under similar conditions yields electronic temperatures of at most 10 °C above room temperature. Thus, the photogeneration of $^1O_2$ by gold NPs proceeds by different mechanisms under different irradiation conditions; the implications for the further development of medical applications of the effect are discussed in detail. Furthermore, we also found that even a moderately thick, but dense, ligand layer significantly reduces the efficiency of $^1O_2$ photogeneration at the NP surface, which also has important consequences for practical applications.

EXPERIMENTAL SECTION

Nanoparticle Preparation. Citrate-stabilized spherical gold NPs with 15 and 46 nm diameter were prepared according to the Turkevich–Frens[28,29] and a seeded growth method,[30] respectively. Gold nanorods (NRods) were synthesized using the seeded-growth method reported by Dickerson et al.[31] with slight modifications. More details of the NP preparation are provided in the Supporting Information. NPs were characterized using UV–vis spectroscopy (Genesys 10 UV), differential centrifugal sedimentation (CPS Instruments DC24000), and transmission electron microscopy (TEM, FEI Tecnai Spirit microscope at 120 kV) (see Figures S1 and S2 in the Supporting Information). The UV–vis absorbance spectrum of NRods showed a transverse plasmon resonance band at 522 nm, and a longitudinal plasmon resonance band at 798 nm and TEM revealed NRods to have a length of 40 nm and a diameter of 12 nm.

Functionalization with thiolated PEG ligands or peptides was achieved by overnight incubation with excess ligand, followed by repeated centrifugation for excess ligand removal. The capping ligands used here were PEG-OH (HS-$(CH_2)_{11}$-$(EG)_4$-OH), mPEG5000 (HS-$(CH_2)_2$-$(EG)_n$-O-CH_3, average MW 5000 g mol^{-1}) and peptide C-TAT (primary sequence CALNNAGRKKRRQRRR); see Figure S3 for the structures of the PEG ligands. More details of the NP functionalization are provided in the Supporting Information.

Singlet Oxygen Detection. $^1O_2$ was detected via the bleaching of 1,3-diphenylisobenzofuran (DPBF), which is widely used for this purpose.[32−35] All experiments involving DPBF were carried out in the dark. Because DPBF is not soluble in neat water,[32] all experiments were conducted in 50/50 (v/v) mixtures of water and ethanol. A fresh solution of DPBF (3.1 mg, 0.115 mM, $A_{412\,nm}$ = 2) in EtOH (100 mL) was kept stirring in the dark. A 10 mm quartz cuvette and a 3 mm stirrer bar were left in aqua regia (1:3 HNO_3:HCl) for 15 min and thoroughly rinsed multiple times with Milli-Q water (MQ H_2O) and EtOH. In the clean cuvette with stirrer bar, either MQ H_2O (600 μL) or NP solution (600 μL) was mixed with the ethanolic dye solution (600 μL). Where appropriate, the NP concentration was adjusted prior to mixing to yield an absorbance of 0.4 at 532 nm in the final solution. The cuvette was sealed with an airtight lid and parafilm, and the UV–vis absorbance spectrum was recorded (Genesys 10 UV). The sample was then placed on a stirring plate (in the dark), and its absorbance spectrum measured every 10 min for 30 min to ensure the solution was stable.

For the irradiation experiments, the cuvette containing 1200 μL of sample solution was placed on a stirring plate in front of the laser. For experiments with NPs, the cuvette was fitted with heat fins using non-silicone heat transfer paste and cooled using a fan. No significant increase of the cuvette temperature beyond a slight warming was observed. For most experiments, the sample was irradiated at 1000 mW (unless stated otherwise) using a 532 nm continuous-wave diode pumped solid state laser (Laser Quantum Opus 532) with a $1/e^2$ beam diameter of 1.85 mm; for some experiments the beam was expanded to 8 mm diameter using a lens, as stated explicitly. The sample was irradiated for 10 min and then removed from the laser setup to record the absorbance spectrum; this was repeated until the sample had been irradiated for 60 min in total. Irradiation of gold NRods in the longitudinal plasmon resonance band at 800 nm was performed in the same setup, but using a titanium:sapphire laser (Coherent Mira 900), aligned on the auxiliary cavity, which prevents mode-locking and thus provides continuous-wave laser operation at 800 nm with 1000 mW power; the beam was expanded to 3.4 mm using two lenses. Pulsed laser irradiation was performed in the same setup, but using the second harmonic of a Q-switched Nd:YAG laser (Quantel Brilliant) (532 nm, 5 ns pulse length, 10 Hz repetition rate, 3.5 mm beam size, 15 mJ pulse energy).

For experiments that included NPs, the absorbance of DPBF at 412 nm was calculated by subtracting the NP absorbance at 412 nm (obtained from neat NP samples) from the measured sample absorbance. The concentration of DPBF in the samples always yielded an initial absorbance very close to 1 at 412 nm; for comparative data analysis, the irradiation-time-dependent DPBF absorbance at 412 nm was therefore normalized to 1 at zero irradiation time.

RESULTS AND DISCUSSION

DPBF Photobleaching. 1,3-Diphenylisobenzofuran (DPBF) readily undergoes a 1,4-cycloaddition on reaction with $^1O_2$ to form endoperoxides which irreversibly yield 1,2-dibenzoylbenzene. DPBF strongly absorbs light at 412 nm (Figure 1a), but due to the loss of the π-system of isobenzofuran, the product does not absorb light at this wavelength; it is this loss of absorbance that is used to detect the presence of singlet oxygen.[36] Here, DPBF was chosen as singlet oxygen sensor as it has no absorbance at 532 or 800 nm, the wavelengths used for laser irradiation of gold nanoparticles in their plasmon resonance bands, and no photobleaching of DPBF was expected to occur upon irradiation in the absence of NPs. Contrary to this expectation, some bleaching was observed under our CW irradiation conditions, with the DPBF absorbance decreasing by ca. 10% upon irradiation at 1 W (37 W cm^{-2}) for 60 min (Figure 1a). As shown in Figure 2a, and described in more detail in the Supporting Information, this photobleaching of DPBF has two phases: (i) a rapid phase, extending over the first 10–20 min of irradiation under the conditions used here, and (ii) a slower phase, which on the time scale investigated appears linear with time. We found that phase i depends on laser power, beam size, and the presence of oxygen, whereas the slope of the time dependent bleaching after 20 min, phase ii, is essentially independent of the presence of oxygen and of the beam power/intensity in the range used here (see Figure S4 for details). It should be noted that similar effects have been reported previously, with CW irradiation at 514 nm for 60 min at significantly lower powers (40 mW) than employed here, leading to a ca. 5% decrease of the absorbance

DOI: 10.1021/acs.jpcc.6b02005
J. Phys. Chem. C 2016, 120, 10647−10657

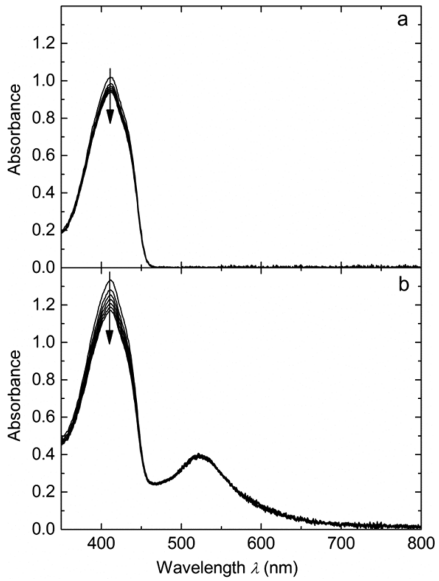

Figure 1. Photobleaching of the DPBF absorbance upon CW irradiation at 532 nm, 1 W (37 W cm^{-2}), in a 50/50 (v/v) mixture of water and ethanol: (a) in the absence of NPs and (b) in the presence of 15 nm citrate-stabilized spherical gold NPs. Shown are absorbance spectra taken at intervals of 10 min from before the irradiation up to a maximum irradiation time of 60 min; the arrows indicate the direction of change.

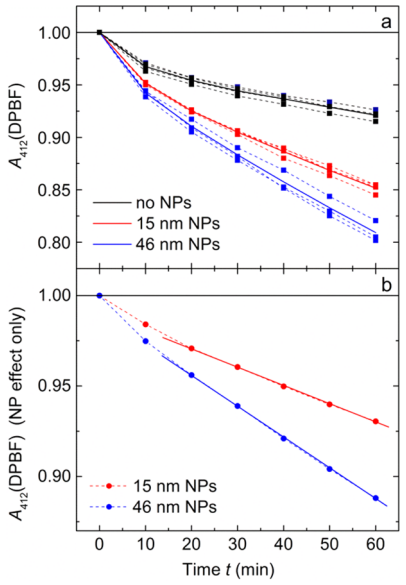

Figure 2. (a) Time dependence of the photobleaching of the DPBF absorbance at 412 nm, A_{412}(DPBF), upon CW irradiation at 532 nm, 1 W (37 W cm^{-2}), in the absence and presence of citrate-stabilized spherical NPs with 15 and 46 nm diameter; shown here are the results from several individual experiments (dashed lines) and the average (solid lines), after subtraction of the NP absorbance and normalization to 1 at time zero; see the Experimental Section for details of data treatment and analysis. (b) Effect of the NPs alone, calculated by subtracting the photobleaching effect of DPBF in the absence of NPs from the results obtained in the presence of NPs; the solid lines in (b) are linear fits of the data in the range 20−60 min.

of DPBF in benzene, although no explanation was suggested in that report.[37] The oxygen dependence of phase i is in agreement with direct photogeneration of singlet oxygen by visible light, which has been suggested to be the reason for DPBF photobleaching upon irradiation with light at wavelengths above 470 nm.[38] However, the slower phase ii is not affected by removing oxygen from the solution (see Figure S4b and Figure 3) and hence cannot be ascribed to singlet oxygen

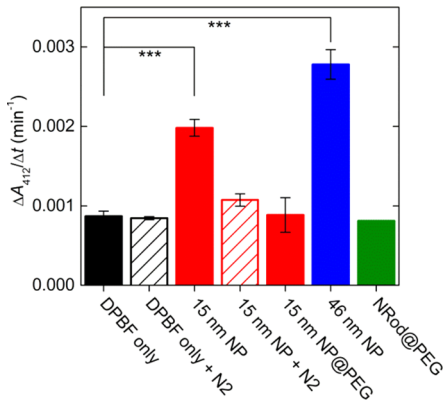

Figure 3. Gradient of the time-dependent DPBF absorbance photobleaching in the irradiation time window 20−60 min for different samples under CW irradiation at 532 nm, 1 W (37 W cm^{-2}). For experiments in the presence of NPs, the NP concentration was adjusted to yield an absorbance of 0.4 at 532 nm. Experiments for DPBF in the absence of NPs and in the presence of 15 nm spherical NPs were also undertaken after bubbling the sample with nitrogen for 10 min, as indicated (+N2). The error bars correspond to the standard deviation of several repeat experiments, and *** indicates statistically significant differences with respect to the experiment on DPBF only, as determined by the ANOVA F-test at $p < 0.001$; it should be noted that the results for 15 or 46 nm spherical NPs without nitrogen bubbling or a PEG capping layer were found to be different to all other results at this statistical significance level. No repeat experiment was undertaken for irradiation of nanorods at 532 nm, but the same result (no additional bleaching in the presence of nanorods) was obtained for irradiation at 800 nm (Figure S5).

formation. At the present moment, the mechanism of both phases of DPBF photobleaching remains unclear, although both effects are highly reproducible and bleaching does not occur when the sample is not exposed to light (see Figure S4a).

Photogeneration of $^1O_2$ by Gold Nanoparticles. In the presence of citrate-stabilized spherical gold NPs, the photobleaching of DPBF upon irradiation at 532 nm, i.e., within the nanoparticle plasmon resonance band, is significantly increased (Figure 1b). The time dependence of the DPBF photobleaching in the absence of NPs and in the presence of NPs with 15 and 46 nm diameter is shown in Figure 2a. Multiple results are shown for each experiment to highlight their reproducibility. It can be clearly seen that the presence of NPs leads to a significant increase of the DPBF photobleaching effect and that larger NPs yield a larger effect although the NP absorbance was adjusted to be the same for all samples, so that the same amount of light was absorbed. The additional photobleaching of DPBF caused by the presence of NPs can be clearly ascribed to the generation of reactive oxygen species (ROS), since purging of the samples with nitrogen removes this effect (see below). Moreover, previous experiments had shown that light irradiation of citrate-stabilized spherical gold NPs leads to the characteristic luminescence of $^1O_2$ at 1280 nm[24] and does not result in the generation of superoxide, O_2^-, or hydroxyl, OH, radicals,[21] which leads us to conclude that the predominant ROS species produced here is singlet oxygen, $^1O_2$.

DOI: 10.1021/acs.jpcc.6b02005
J. Phys. Chem. C 2016, 120, 10647−10657

The fact that significant DPBF photobleaching occurs even in the absence of NPs requires careful consideration for the analysis of these data. Like DPBF photobleaching in the absence of NPs, the effect in the presence of NPs shows two phases. However, subtraction of the effect observed when only the dye is present yields an essentially linear time dependence for the additional effect ascribed to the NPs on the time scale of the experiment (Figure 2b), indicating that the NP-induced photogeneration of $^1O_2$ is essentially constant over our experimental time interval. Moreover, the second phase of direct DPBF photobleaching is largely independent of the laser power, at least down to 0.1 W, i.e., significantly lower powers than those used for most of the experiments reported here, as shown in detail in the Supporting Information (Figure S4a), and therefore should be independent of the presence of NPs whose absorbance leads to a decrease of the laser power along the beam path, allowing a direct comparison of the results obtained in the time frame of 20−60 min. Moreover, this slower phase of direct DPBF photobleaching is also independent of the presence of oxygen. For these reasons, only data starting at 20 min irradiation will be used for quantitative comparisons.

Figure 3 summarizes the main results obtained here after NP photoexcitation at 532 nm. It is very obvious that citrate-stabilized spherical gold NPs induce significantly faster DPBF photobleaching than is observed in their absence (black); this is found for 15 nm gold nanoparticles (red) but is even more pronounced for larger NPs with 46 nm diameter (blue). Increasing the size of the spherical NPs from 15 to 46 nm increases the NP-induced DPBF photobleaching (i.e., the additional effect, after subtracting the direct DPBF photobleaching effect) by ca. 40%, indicating more $^1O_2$ formation. It is interesting to note that unlike the direct DPBF photobleaching, which is not affected by nitrogen purging, the NP-induced additional bleaching is significantly reduced by nitrogen purging, almost down to the level of the direct DPBF photobleaching effect. This strongly supports the conclusion that the NP-induced effect is caused by the formation of $^1O_2$ which then leads to DPBF photobleaching. Furthermore, capping the 15 nm gold NPs with PEG-OH, a moderately large ligand (Figure S3), essentially removes the NP-induced bleaching and reduces the observed effect to the level of the direct DPBF photobleaching.

Gold nanorods (NRods) with a length of 40 nm and a diameter of 12 nm, which have two plasmon resonance bands, namely the transverse band at 522 nm and the longitudinal one at 798 nm (Figure S1a), stabilized with a capping layer consisting of a mixture of a PEG polymer (mPEG5000) and a peptide (C-TAT) (see the Experimental Section), were also investigated. Irradiation at 532 nm, i.e., in the transverse plasmon resonance band, showed no additional DPBF bleaching above the direct DPBF effect (Figure 3). Irradiation with 1 W (11 W cm^{-2}) CW laser power at 800 nm, i.e., in the longitudinal plasmon resonance band (Figure S5), showed reduced direct DPBF photobleaching compared to irradiation at 532 nm, but again no additional photobleaching was observed in the presence of NRods. These results show that the NRods used here, which have a ligand layer consisting of a mixture of a PEG polymer and a peptide, do not induce the formation of $^1O_2$ upon laser irradiation, independent of the plasmon resonance which is photoexcited.

Irradiation at 532 nm in the presence and absence of citrate-stabilized spherical gold NPs with 15 nm diameter was also investigated using laser pulses with a pulse duration of 5 ns (Figure 4). In this case, the UV−vis spectra show a slight

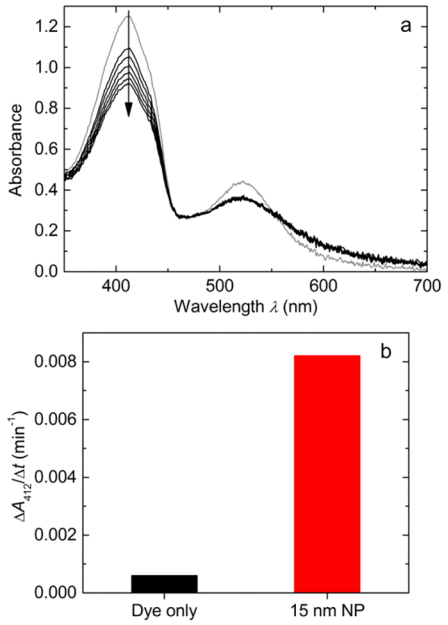

Figure 4. Photobleaching of the DPBF absorbance upon laser irradiation with 5 ns laser pulses at 532 nm, 0.15 W, 10 Hz repetition rate (corresponding to a power density of 1.5 W cm^{-2} and a pulse energy density of 0.15 J cm^{-2}). (a) Absorbance spectra in the presence of citrate-stabilized spherical gold NPs with 15 nm diameter, taken at intervals of 5 min from before the irradiation (gray) up to a maximum irradiation time of 30 min; the arrow indicates the direction of change. (b) Gradient of the time-dependent DPBF photobleaching (measured at 412 nm) in the irradiation time window of 20−30 min in the absence and presence of NPs.

broadening of the NP plasmon resonance band at 520 nm during the first 5 min of irradiation, suggesting that some aggregation occurs; after the initial 5 min, however, the NPs remain stable. Analysis of the spectra shows that photobleaching of DPBF in the absence of gold NPs is similar to the results obtained using CW laser irradiation at comparable average powers (Figure S4a). In the presence of gold NPs with 15 nm diameter, on the other hand, the NP-induced bleaching effect (i.e., the effect remaining after subtracting the direct DPBF photobleaching effect) which is induced by pulsed laser irradiation is larger than that caused by CW irradiation by almost 1 order of magnitude, in spite of the significantly lower laser power employed during the pulsed irradiation experiments (0.15 W vs 1 W), which leads to a correspondingly lower number of absorbed photons; compare Figure 4b (pulsed irradiation) with Figure 3 (CW irradiation).

Quantum Yield of $^1O_2$ Photogeneration. It is straightforward to estimate the quantum yield of NP-induced DPBF photobleaching from the absorbed laser power and the observed rate of absorbance bleach. For the citrate-stabilized spherical NPs with 15 and 46 nm diameter under CW irradiation at 532 nm, this yields values of 5×10^{-7} and 8×10^{-7}, respectively. Thus, less than one of each 1 million photons absorbed by a NP leads to the photobleaching of a DPBF molecule under CW irradiation. For irradiation of 15 nm NPs with 5 ns laser pulses, on the other hand, the quantum yield of NP-induced DPBF photobleaching is 3.5×10^{-5}, i.e.,

DOI: 10.1021/acs.jpcc.6b02005
J. Phys. Chem. C 2016, 120, 10647−10657

almost 2 orders of magnitude larger than for CW irradiation, but still very small.

Diffusion of oxygen[39] over the lifetime of $^1O_2$ (approximately 6 μs in 50/50 water/ethanol[32]) covers a distance larger than the average distance between DPBF molecules at the concentrations used here, and hence it can be concluded that a significant fraction of the photogenerated $^1O_2$ which escapes from the NP surface should be detected. This is confirmed by literature reports showing that a DPBF concentration of ca. 10^{-4} M, which is close to the concentration used here, is sufficient to detect 50% of photogenerated $^1O_2$.[32] Thus, the observed low quantum yield of DPBF photobleaching indicates a very low quantum yield of $^1O_2$ photogeneration by gold NPs (i.e., number of $^1O_2$ generated for each photon absorbed), having values of the order of ca. 10^{-6} for CW irradiation and ca. 10^{-4} for irradiation with nanosecond laser pulses.

Mechanism of $^1O_2$ Photogeneration by Gold Nanoparticles. Our results show that irradiation of citrate-stabilized spherical gold NPs at 532 nm, i.e., in their surface plasmon band, with pulsed or CW laser light leads to the production of $^1O_2$, detected here by monitoring the bleaching of DPBF absorbance. However, the rate of $^1O_2$ production is much larger when using short laser pulses than when using CW light of comparable intensity. Whereas ca. 24% of the dye is bleached after only 10 min of irradiation of 15 nm NPs with 5 ns laser pulses at an average power of 150 mW (Figure 4), only 1−2% of the dye is bleached over this time by irradiation of the same NPs with CW light at significantly higher power (1 W) (Figure 2). This difference allows one to draw important conclusions on the mechanism of $^1O_2$ production by irradiation of gold nanoparticles.

Pulsed Irradiation: Heating of Nanoparticles. Irradiation of spherical gold NPs at 532 nm leads to the excitation of their plasmon resonance, which can be described as a coherent oscillatory motion of the conduction band electrons; this oscillation dephases and decays on the sub-100 fs time scale, with only a very small radiative contribution, so that most of the excitation energy is retained as electronic excitation in the form of electron−hole pairs. Since the photon energy is close to the minimum energy required for direct excitation of d-band electrons into the conduction band of gold, a minor contribution of this excitation mechanism cannot be ruled out; however, d-band holes are filled by conduction band electrons on the 10 fs time scale, yielding essentially the same outcome as excitation of the plasmon resonance band.[25] The excited electrons initially have a nonthermal energy distribution, and often are referred to as "primary hot electrons", although the concept of temperature does not strictly apply to such a distribution. They rapidly (within less than 500 fs) equilibrate by electron−electron scattering to yield a Fermi distribution corresponding to an elevated temperature and can then be referred to as "hot electrons".[25−27] Hot electrons have been shown to cause gold−thiol bond dissociation at the surface of gold NPs[40] and have been suggested to be responsible for the creation of $^1O_2$ by irradiation of gold NPs with nanosecond laser pulses.[24] They lose their energy on the time scale of a few picoseconds by interaction with the lattice (electron−phonon scattering) with coupling times that are essentially size-independent for NPs above 10 nm in diameter, although they strongly depend on the amount of energy deposited due to the temperature-dependent electronic heat capacity.[25,26] Because the lattice heat capacity is much larger than the electronic heat capacity, this leaves the electrons and the lattice in equilibrium at a temperature which is significantly lower than the initial electronic temperature; finally, cooling occurs by heat transfer to the solvent and heat diffusion on the time scale of 10 to a few 100 ps, strongly depending on NP size.[41]

Since the dissipation of the absorbed energy proceeds on the picosecond time scale, excitation with a nanosecond laser pulse yields a highly nonequilibrium situation during the duration of the laser pulse where energy is continuously deposited into the electronic system and at the same time flows through the lattice into the surrounding solvent. It is therefore not straightforward to predict the temperature of the hot electrons achieved in such experiments. We used the "two-temperature model" for the electron and phonon heat baths[25,26,42,43] coupled to finite-element heat transfer and diffusion simulations in the surrounding solvent to estimate this temperature; details of these simulations are given in the Supporting Information. As shown in Figure 5, under our conditions the electrons are

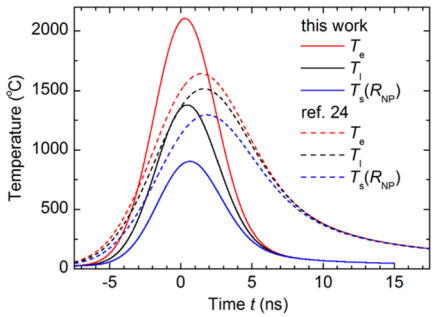

Figure 5. Time-dependent temperatures of the conduction band electrons (red), lattice (black), and first solvent layer (blue), calculated for our experiments using nanosecond-laser pulse excitation (15 nm spherical NPs in 50/50 EtOH/water, 5 ns laser pulses with 0.15 J cm^{-2} intensity, solid lines) and for the experiments described in ref 24 (40 nm spherical NPs in 80/20 EtOH/water, 7 ns laser pulses with 0.03 J cm^{-2} intensity, dashed lines) using the "two-temperature model" for the electron and phonon heat baths, coupled to finite-element heat transfer and diffusion simulations in the surrounding solvent (see Supporting Information for details); time zero corresponds to the center of the laser pulse.

expected to reach a temperature of 2100 °C, whereas the lattice reaches temperatures of the order of 1400 °C and the solvent in the immediate vicinity of the NP a temperature of about 900 °C.

A lattice temperature of 1400 °C, which is above the melting temperature for solid gold, albeit present for only a few nanoseconds, might be sufficient to cause temporary melting of the nanoparticle,[25] although the pulse intensities used here are still below the reported threshold for size reduction of gold NPs of 15 nm diameter by nanosecond laser pulses.[44] Nevertheless, a minor effect on the shape and/or size of the NPs, especially at the upper end of the size distribution, cannot be ruled out and may be related to the minor NP spectral changes observed upon irradiation which suggest some aggregation to occur (see above). Because of the slower heat dissipation around larger NPs, these are heated to higher temperatures and hence are more likely to fragment, in agreement with experimental results on nanosecond-laser pulse induced fragmentation, which also show that fragmentation is finished after 5 min under conditions similar to the ones used here.[44] Since our NPs were prepared without excess citrate, the resulting increase in

DOI: 10.1021/acs.jpcc.6b02005
J. Phys. Chem. C 2016, 120, 10647−10657

the ratio of surface area to volume may indeed cause some aggregation. It also cannot be ruled out that the solvent near the NP surface temporarily forms bubbles,[45] although the pulse intensities used here are still below the reported threshold for bubble formation by nanosecond pulses for 15 nm NPs.[46] Such bubbles could lead to better thermal insulation, thus potentially increasing the maximum temperatures, but on the other hand, they might prevent oxygen from reaching the NP surface, thus reducing the chance of $^1O_2$ formation.

Pulsed Irradiation: $^1O_2$ Photogeneration by Equilibrated Hot Electrons. The formation of $^1O_2$ from the triplet ground state by interaction with a photoexcited sensitizer requires a change of the electron spin and hence cannot result from dipole−dipole (Förster) interaction, but only from Dexter-type electron exchange coupling; the latter can be described as simultaneous transfers of an electron from one of the $2\pi^*$ molecular orbitals on oxygen to a photogenerated hole on the sensitizer and of an electron with opposite spin from a high-energy excited sensitizer level to the same or the other $2\pi^*$ orbital, resulting in the formation of the $^1\Sigma$ or $^1\Delta$ singlet oxygen state, respectively.[47] This mechanism requires significant overlap of the relevant electronic wave functions and hence only occurs at short distances of at most 10 Å. Since the photoexcited hot electrons have such a short lifetime, this reaction can only occur if an oxygen molecule happens to be in the vicinity of the NP or is temporarily adsorbed to its surface at the moment of excitation. A similar reaction occurs on photoexcited Si nanocrystals,[37,47] although in this case the reaction is more efficient than for Au NPs due to the much longer lifetime of the photoexcited excitons in Si. Thus, the short lifetime of hot electron excitation in gold nanoparticles easily explains the low quantum yield of $^1O_2$ photogeneration which is observed here.

The excitation of electrons to temperatures exceeding 2000 °C means that a significant number have sufficient energy to excite an oxygen molecule to the $^1\Delta$ state, which has an energy of 0.98 eV above the $^3\Sigma$ ground state[23] (see Figure 6). The

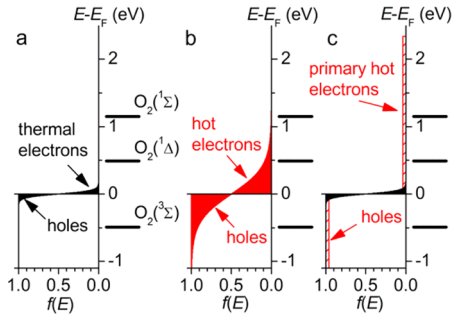

Figure 6. Schematic diagram showing the population probability $f(E)$ for a NP electron state at energy E near the Fermi level, E_F, under different conditions: (a) in equilibrium at room temperature, (b) at an electron temperature of T_e = 2100 °C after electron−electron equilibration ("hot electrons"), and (c) immediately after the absorption of photons by single electrons ("primary hot electrons", with population changes highly exaggerated to make them visible). Also shown are the energies of the ground-state triplet ($^3\Sigma$) and lowest-excited singlet state ($^1\Delta$) of oxygen as well as the next singlet state ($^1\Sigma$) under the assumption that E_F is equidistant from the $^3\Sigma$ and $^1\Delta$ energies. Excitation of an oxygen molecule to $^1O_2$ requires the simultaneous transfer of an electron from the oxygen to a hole at the energy of the $^3\Sigma$ state and of a hot electron with the opposite spin and an energy at the $^1\Delta$ (or $^1\Sigma$) level to the oxygen molecule.

number of hot electrons available at the higher energy—and the number of holes available at the lower energy involved in this two-electron exchange reaction—can be estimated from the density of states of gold and the Fermi distribution, as described in more detail in the Supporting Information. For example, for a spherical NP with 15 nm diameter at an electron temperature of 2100 °C, there are 260 electrons within an energy interval of 0.1 eV around the $^1\Delta$ state. (It should be noted that the relevant energy interval is the width of this state for an oxygen in the vicinity or temporarily adsorbed onto a NP, which is not known, so only relative numbers will be used here.) Thus, the electron temperatures achieved in our experiment are sufficient for a significant population of hot electrons and holes at the relevant levels.

The large number of equilibrated hot electrons available during a nanosecond-laser pulse also rules out the primary hot electrons as the main source of $^1O_2$ photogeneration. The number of primary hot electrons available during the pulse duration can be estimated from the number of photons which are absorbed per nanosecond, multiplied by their lifetime, which is less than 500 fs.[26] However, these primary hot electrons populate NP states at energies from the Fermi level E_F to E_F + 2.34 eV (the energy of a photon at 532 nm) (see Figure 6c). For 15 nm NPs and excitation with 5 ns laser pulses with 0.15 J cm^{-2} intensity, this predicts that not more than three primary hot electrons are available within an energy interval of 0.1 eV around the $^1\Delta$ level at any time during the laser pulse, assuming that all levels are equally populated and taking into account that the density of states for gold has an essentially constant value in the relevant energy range around E_F.[48] This is significantly less than the number of hot (equilibrated) electrons available at the maximum electron temperature, which was estimated to be on the order of 260 for the same energy interval (see above). Thus, we can conclude that it is indeed the hot electrons which are responsible for the observed $^1O_2$ photogeneration when using short laser pulses for excitation.

Similar results to those obtained here using pulsed irradiation have recently been reported for spherical gold NPs with 40 nm diameter.[24] Although a significantly lower laser pulse energy density (0.03 J cm^{-2}, compared to 0.15 J cm^{-2} here) was used under otherwise similar experimental conditions, slightly faster $^1O_2$ photogeneration was observed in this study, with the DPBF absorbance decreasing by ca. 40% over 10 min of irradiation, compared to the ca. 24% decrease observed here in the first 10 min (Figure 4a). In this context, it is interesting to note that in spite of the lower laser pulse energy density the NPs are heated to almost the same electron temperature as in our experiments (see Figure 5). This is largely due to (i) heat dissipation from larger NPs being slower[41] and (ii) the use of 80/20 EtOH/water as solvent in ref 24, which has slower heat transport than a 50/50 EtOH/water mixture. An explicit calculation of the number of hot electrons available at the energy of the oxygen $^1\Delta$ state for the two experiments is given in the Supporting Information; together with a detailed consideration of all other experimental differences, these numbers yield very good agreement between the expected and the observed relative $^1O_2$ photogeneration rates (see the Supporting Information for details). This provides further support for the conclusion that $^1O_2$ photogeneration is mediated by the equilibrated hot electrons of gold nanoparticles under nanosecond-pulsed laser irradiation.

DOI: 10.1021/acs.jpcc.6b02005
J. Phys. Chem. C 2016, 120, 10647−10657

Continuous Irradiation: $^1O_2$ Photogeneration by Primary "Hot" Electrons. Compared to the effect of pulsed irradiation, the rate of $^1O_2$ photogeneration is much smaller when using CW light of comparable intensity. Whereas ca. 24% of the dye is bleached after only 10 min of irradiation of spherical NPs with 15 nm diameter with 5 ns laser pulses at an average power of 150 mW (Figure 4), only 1−2% of the dye is bleached over this time by irradiation of the same NPs with CW light at significantly higher power (1 W) (Figure 2). In a previous publication,[24] significantly higher rates of DPBF photobleaching had been reported under conditions which appear to be similar to the ones used here. In this context, we note that we also observed such significantly higher rates of bleaching, but only when the sample preparation protocol described in the Experimental Section was not followed accurately; for example, the use of dye solution that had not been freshly prepared or of a cuvette that had not been cleaned thoroughly and rinsed multiple times with MQ water or the use of a cell that was not sealed during irradiation, leading to some loss of ethanol from the solution, all resulted in larger and highly irreproducible bleaching of DPBF under CW irradiation, up to levels comparable to those reported in ref 24, even in the absence of NPs.

In the following, we will show that photogeneration of $^1O_2$ under CW irradiation, unlike pulsed irradiation, is mediated by the initially created "primary hot" electrons; i.e., it occurs during the short time during which the excited electrons have not yet relaxed to a thermal distribution (see Figure 6c). Under the CW irradiation conditions used here (1 W, 1.85 mm beam diameter), a spherical NP with 15 nm diameter absorbs photons at an average rate of 1.3×10^8 s^{-1}, as estimated from the absorption cross section[49] and the beam intensity. This means that after absorption of a photon there is enough time for full relaxation and transfer of the photon energy into the solvent, which occurs in less than 100 ps,[41] before absorption of the next photon. Absorption of one photon by a 15 nm NP yields "hot" electrons at a temperature of 10 K above the surrounding after electron−electron equilibration; these "hot" electrons lose their energy by electron−phonon scattering within a few picoseconds to yield a NP whose temperature is only 80 mK above the surrounding. Neither of these effects is expected to yield any significant photochemical effects; estimates analogous to those described above predict that for a spherical 15 nm NP with an electron temperature of 35 °C there are ca. 2.6×10^{-5} electrons within an energy interval of 0.1 eV around the oxygen $^1\Delta$ state and the same number of holes around the $^3\Sigma$ state energy. This means that there are on the order of 10^7 times less hot electrons and 10^7 times less holes available for the photoreaction than under our pulsed laser irradiation conditions, which rules out any significant reaction; this is also confirmed by the fact that these population numbers are less than a factor 2 larger than those for room temperature, where no $^1O_2$ is generated in the absence of light.

This leaves only the primary hot electrons, i.e., those electrons that are excited upon absorption of a photon but have not yet equilibrated by electron−electron scattering, as potential cause for photogeneration of $^1O_2$. Absorption of a single photon can potentially excite electrons to energies of up to 2.34 eV above the Fermi level. If one assumes excitation of only one electron by each photon and equal excitation probability for all available electrons, as shown in Figure 6c, on average there will be 0.043 electrons within an energy interval of 0.1 eV around the oxygen $^1\Delta$ state, which is approximately 5000 times less than during a single laser pulse in the pulsed experiments, see above. Taking into account that the same factor also applies to the holes required for the Dexter mechanism, but correcting for the lifetime of the excitation (500 fs for primary hot electrons created during CW irradiation,[25−27] ca. 3 ns for the hot electron distribution induced by a single laser pulse; see Figure S6) and the repetition rates (1.3×10^8 s^{-1} for single photon absorption during CW irradiation, 10 s^{-1} for the pulsed laser irradiation), one would predict a rate of $^1O_2$ photogeneration under our CW irradiation conditions which is smaller than that expected for our pulsed irradiation conditions by a factor on the order of 10^4. This is significantly closer to the experimental results (ratio of $^1O_2$ photogeneration rates under pulsed vs CW irradiation of 10−20) than any estimate based on the equilibrated "hot" electrons after the absorption of a single photon. The main discrepancy between the predicted and observed CW results arises from the assumption of direct excitation of single electrons in the above estimate, which is not valid for irradiation at 532 nm, i.e., in the gold NP plasmon resonance band, since this leads to the coherent excitation of many electrons which rapidly dephases without the electrons exchanging energy. Thus, absorption of a single photon yields more than one primary hot electron, with the photon's energy distributed over all of them. Consequently, the energy distribution even of the primary hot electrons will not extend up to 2.34 eV above E_F but will be shifted toward the states nearer the Fermi level, thus increasing the population of states around the oxygen $^1\Delta$ energy and hence the yield of $^1O_2$. A more quantitative estimate of this effect is beyond the scope of this paper.

An alternative possibility for the mechanism of $^1O_2$ photogeneration by gold NPs could be envisaged, which is based on increased direct photoexcitation of oxygen due to the well-known local electric field enhancement in the vicinity of metal NPs by the plasmon electrons. However, significant field enhancement extends to distances comparable to the dimensions of the nanoparticle,[50] so that this mechanism is in disagreement with our observation that a PEG-OH capping layer, which has a thickness of only 2 nm,[51] completely inhibits $^1O_2$ photogeneration (Figure 3). Dexter-type electron exchange coupling, on the other hand, is known to be of significance only over distances of less than 1 nm, as discussed above, and thus is further supported by this observation.

In conclusion, CW irradiation is less efficient than pulsed laser irradiation in photogenerating $^1O_2$ since the (equilibrated) hot electrons, which are the main mediator of the photochemistry in the case of pulsed irradiation, do not have sufficient energy/temperature to drive $^1O_2$ photogeneration. Nevertheless, our results confirm that CW irradiation of spherical gold NPs produces detectable amounts of $^1O_2$.[19,24] The absence of significant amounts of (equilibrated) hot electrons means that $^1O_2$ photogeneration proceeds via a different mechanism under CW irradiation compared to pulsed laser generation; the above estimates indicate that it is the primary hot electrons, i.e., the directly photoexcited electrons, which are responsible for the photochemistry here and that the photochemical reaction must occur before these equilibrate by electron−electron thermalization.

Design Considerations for Medical Applications. Photodynamic therapy holds great promises for medical applications, such as the treatment of cancer, because of the ability to selectively affect diseased tissue only.[22,23] However,

DOI: 10.1021/acs.jpcc.6b02005
J. Phys. Chem. C 2016, 120, 10647−10657

wider use of photodynamic cancer therapy is currently prevented by several limitations imposed by the available photosensitizers. These limitations include toxicity, poor stability and photostability, poor selectivity for cancer tissue, and the need of using visible light with poor tissue penetration. All of these limitations, in principle, can be overcome by the use of gold nanoparticles, which are nontoxic, have excellent stability even under irradiation, can target cancer tissue either passively by the enhanced penetration and retention (EPR) effect[52,53] or by active targeting,[10,11] have extinction coefficients that are larger than those of dye molecules by several orders of magnitude, and can be tuned to absorb in the near-infrared spectral region for maximum tissue penetration.

Gold nanoparticles have been reported to have three potential modes of operation for inducing cell death by irradiation, namely (i) hyperthermia, which is based on the rapid conversion of the absorbed light energy into heat, (ii) NP-assisted photodynamic therapy, in which the efficiency of a standard sensitizer is amplified by the NP plasmon field enhancement effect, or (iii) a direct photochemical mechanism without involvement of a photosensitizer.

The feasibility of photothermal therapy has been clearly established by careful experiments *in vitro*[11−13,15,54] and has been shown to work *in vivo*.[14,17,31,55,56] However, it should be noted that most studies reporting successful photothermal therapy made no attempt to either confirm significant heating or rule out photochemical effects, which means that some of these reported results could in fact arise from photochemical rather than photothermal effects or from a synergistic combination of photochemical and photothermal effects.[13,17,20,57] As has been pointed out recently,[17] another problem with many reports on photoinduced hyperthermia using NPs is the relatively high light intensity required to reach sufficient temperatures, which often were well above the generally accepted skin tolerance threshold.

The presence of gold NPs can also lead to increased photogeneration of $^1O_2$ by traditional photodynamic sensitizers,[58−62] which can be ascribed to the local electric field enhancement in the vicinity of metal NPs by the plasmon electrons, similar to the well-studied SERS (surface-enhanced Raman spectroscopy) effect. This approach might help to alleviate some of the drawbacks of traditional photodynamic therapy but does not directly overcome them, since it still requires the presence of a sensitizer. In fact, the requirement for two active components, gold NP and sensitizer, which must be colocalized, introduces an additional complication, and care must be taken to avoid a reduction of the photosensitizer effect due to quenching of its excited state by the metal NP.[60]

In an alternative approach, cell death has been demonstrated to occur following irradiation of intracellular (endocytosed) gold NPs even at irradiation levels that are not high enough to cause significant heating.[16−18] This photochemical effect has been related to the observation that irradiation of NPs *in vitro* results in the formation of singlet oxygen,[17−20,24,63] which is the active species in traditional photodynamic therapy. Because of the short lifetime of $^1O_2$ (3.4 μs in water[64]), its action is highly localized—an oxygen molecule only diffuses[39] over the length scale of 100 nm in this time. For this reason, only intracellular NPs are expected to trigger cell death by the photochemical route, although they may initially be located inside endosomes which are known to be broken up by NPs under CW irradiation.[16] On the other hand, the localization of the photochemical effects within individual cells also means that in situations where different types of cells coexist in close vicinity, selective targeting of particular cells and minimization of collateral damage should be achievable. This is different than photothermally induced cell death, which affects all cells within the irradiated volume more or less indiscriminately, as long as some of them contain NPs, because of the fast diffusion of heat over the relevant length scales.

The results of the experiments described here provide more insight into the direct photochemical mechanism and allow some important conclusions to be made for the further development of practical applications. They show that detectable amounts of $^1O_2$ are generated by irradiation of NPs with short laser pulses or CW light even in the absence of a photodynamic sensitizer, albeit with low quantum yield. Short laser pulses are significantly more efficient at this process, since they can heat a significant fraction of the NP conduction band electrons to high enough temperatures to excite oxygen to the singlet state. However, this requires pulse energy densities that are well above generally accepted safe levels for the irradiation of skin with pulsed laser light. Since the effect requires the absorption of many photons by a NP during one laser pulse, it is highly nonlinear with respect to irradiation intensity, and thus it will not be possible to compensate lower irradiation levels by longer irradiation times. Furthermore, pulsed irradiation at the required intensities also can cause other effects, such as NP fragmentation[25,44] or bubble formation,[45,46] and it is not clear what consequences these effects may have when occurring in tissue. Although the use of femtosecond laser pulses, as compared to the nanosecond pulses used here, might alleviate some of these problems to some extent, they would require even more sophisticated equipment which may not be suitable for a clinical environment.

The use of CW light, on the other hand, is straightforward and does not even require a laser but can be achieved with simple lamps. In spite of the lower quantum yield of $^1O_2$ photogeneration by NPs under CW irradiation which is reported here, cell death induced by CW light in the presence of NPs has been reported *in vitro* and *in vivo*.[16,17] Although the experiments described here, which did not involve any biological material, were undertaken at light intensities that are above safe irradiation levels, the mechanism of $^1O_2$ photogeneration by NPs under CW illumination is shown to be based on the absorption of single photons. This means that lower light intensities can be compensated for by longer irradiation times, allowing one to reduce the intensity to safe levels for biological or medical applications without affecting the amount of $^1O_2$ generated. $^1O_2$ photogeneration and cancer cell destruction *in vitro* and *in vivo* have indeed been observed upon irradiation on the minute time scale at intensities below safe levels and using nonlaser light sources.[17,19,20]

The results presented here indicate another design criterion which needs to be fulfilled for successful implementation of the photochemical route of inducing cell death by irradiation of NPs, namely that the NPs must not possess a dense capping layer. Even the thin capping layer formed by PEG-OH, with a thickness of only 2 nm,[51] is sufficient to completely inhibit $^1O_2$ photogeneration (Figure 3). This is in full agreement with the suggestion that energy exchange between the NP and the oxygen molecule occurs via the Dexter (two electron exchange) mechanism, which is limited to distances of less than 1 nm. Similar effects have been reported for $^1O_2$ photogeneration by Si nanocrystals, which is significantly affected by a thin oxide layer.[37,47] It is important to point out that the assay used here

DOI: 10.1021/acs.jpcc.6b02005
J. Phys. Chem. C 2016, 120, 10647−10657

for $^1O_2$ detection (bleaching of DPBF) only reports on singlet oxygen found outside the NP capping layer; thus, it cannot be ruled out that even on NPs with a PEG-OH capping layer some $^1O_2$ is photogenerated at the NP surface but reacts with the NP ligands and hence is quenched. On the other hand, such singlet oxygen would not be of any direct use for practical applications, such as the induction of cell death, so that the assay results in fact report the effects relevant for such applications. Uncapped (citrate) NPs are rapidly covered by a protein corona after they have been taken up into live cells,[65] but it appears that this corona is permeable enough for oxygen to not completely prevent singlet oxygen formation, as evidenced by fact that cell death by the photochemical route has been observed with such NPs;[16] it may be that because of their size proteins are not able to form a capping layer (corona) of similar density as the smaller ligands used here. Similarly, a lipid bilayer appears to allow oxygen access to the surface of gold nanorods,[17] whereas a dense pentapeptide (CALNN) capping layer on spherical gold nanoparticles is sufficient to suppress the photochemical mechanism of cell death.[66]

It also seems likely that the thick PEG capping layer present on the nanorods used here is the main reason for the absence of $^1O_2$ photogeneration by nanorods upon irradiation in either the transversal or the longitudinal plasmon resonance band that was observed here. Because of their longitudinal plasmon resonance band, which is in the near-IR spectral region with high tissue penetration, nanorods are more suitable for practical photodynamic applications in tissue. However, standard synthesis protocols yield nanorods within a bilayer of cytotoxic CTAB, so that ligand exchange is required before any biological or medical application, and care will need to be taken to choose suitable ligands to allow access of oxygen to the nanorod surface. Potential examples for these are poly(vinylpyrrolidone), lipid bilayers, or mesoporous silica, all of which have been used successfully in experiments showing photochemically induced cell death using gold nanorods.[17,18,60]

CONCLUSIONS

DPBF has been used successfully to detect singlet oxygen that is formed when spherical NPs are irradiated at 532 nm, either with CW or pulsed laser irradiation. Singlet oxygen generation by pulsed laser irradiation has been shown to act via the equilibrated hot electrons that can reach temperatures of several thousand degrees during the laser pulse; CW irradiation, on the other hand, can act only via the directly excited primary "hot" electrons, which rapidly lose their energy by electron−electron equilibration, and hence is significantly less efficient for the formation of singlet oxygen. Nevertheless, even CW irradiation can produce enough singlet oxygen for photodynamic therapy applications and will allow practical applications of the effect at safe irradiation levels. Photodynamic therapy using gold nanoparticles will also require careful design of the nanoparticles with respect to size, shape, and capping layer and will require internalization of the NPs, not just attachment to the cell surface, which is sufficient for photothermal therapy.

ASSOCIATED CONTENT

Supporting Information

The Supporting Information is available free of charge on the ACS Publications website at DOI: 10.1021/acs.jpcc.6b02005.

S1: Nanoparticle preparation and characterization; S2: Ligands used for the preparation of PEG-capped nanoparticles; S3: DPBF photobleaching results; S4: Results of irradiation of gold nanorods at 800 nm; S5: Simulation of the heat dissipation dynamics during irradiation with nanosecond laser pulses; S6: Simulation of the hot electron density during irradiation with nanosecond laser pulses; S7: Comparison of the results of pulsed irradiation observed here and by Pasparakis (2013) (PDF)

AUTHOR INFORMATION

Corresponding Author

*Tel +44-151-794 3317; e-mail m.volk@liverpool.ac.uk (M.V.).

Notes

The authors declare no competing financial interest.

ACKNOWLEDGMENTS

This research was supported by funding from the European Research Council (ERC Advanced Grant PANDORA), the Engineering and Physical Sciences Research Council (DTP Studentship, S.J.C.), and the Egyptian Ministry of Higher Education (Joint Supervision program Award, D.S.).

REFERENCES

(1) Boisselier, E.; Astruc, D. Gold Nanoparticles in Nanomedicine: Preparations, Imaging, Diagnostics, Therapies and Toxicity. *Chem. Soc. Rev.* **2009**, *38*, 1759−1782.

(2) Reddy, L. H.; Arias, J. L.; Nicolas, J.; Couvreur, P. Magnetic Nanoparticles: Design and Characterization, Toxicity and Biocompatibility, Pharmaceutical and Biomedical Applications. *Chem. Rev.* **2012**, *112*, 5818−5878.

(3) Lin, M.; Zhao, Y.; Wang, S.; Liu, M.; Duan, Z.; Chen, Y.; Li, F.; Xu, F.; Lu, T. Recent Advances in Synthesis and Surface Modification of Lanthanide-Doped Upconversion Nanoparticles for Biomedical Applications. *Biotechnol. Adv.* **2012**, *30*, 1551−1561.

(4) Otsuka, H.; Nagasaki, Y.; Kataoka, K. PEGylated Nanoparticles for Biological and Pharmaceutical Applications. *Adv. Drug Delivery Rev.* **2012**, *64*, 246−255.

(5) Sperling, R. A.; Rivera Gil, P.; Zhang, F.; Zanella, M.; Parak, W. J. Biological Applications of Gold Nanoparticles. *Chem. Soc. Rev.* **2008**, *37*, 1896−1908.

(6) Dykman, L.; Khlebtsov, N. Gold Nanoparticles in Biomedical Applications: Recent Advances and Perspectives. *Chem. Soc. Rev.* **2012**, *41*, 2256−2282.

(7) Huang, X. H.; Jain, P. K.; El-Sayed, I. H.; El-Sayed, M. A. Gold Nanoparticles: Interesting Optical Properties and Recent Applications in Cancer Diagnostic and Therapy. *Nanomedicine* **2007**, *2*, 681−693.

(8) Chithrani, B. D.; Ghazani, A. A.; Chan, W. C. W. Determining the Size and Shape Dependence of Gold Nanoparticle Uptake into Mammalian Cells. *Nano Lett.* **2006**, *6*, 662−668.

(9) Nativo, P.; Prior, I. A.; Brust, M. Uptake and Intracellular Fate of Surface-Modified Gold Nanoparticles. *ACS Nano* **2008**, *2*, 1639−1644.

(10) Loo, C.; Lowery, A.; Halas, N. J.; West, J.; Drezek, R. Immunotargeted Nanoshells for Integrated Cancer Imaging and Therapy. *Nano Lett.* **2005**, *5*, 709−711.

(11) El-Sayed, I. H.; Huang, X. H.; El-Sayed, M. A. Selective Laser Photo-Thermal Therapy of Epithelial Carcinoma Using Anti-EGFR Antibody Conjugated Gold Nanoparticles. *Cancer Lett.* **2006**, *239*, 129−135.

(12) Huang, X.; El-Sayed, I. H.; Qian, W.; El-Sayed, M. A. Cancer Cell Imaging and Photothermal Therapy in the Near-Infrared Region by Using Gold Nanorods. *J. Am. Chem. Soc.* **2006**, *128*, 2115−2120.

(13) Kah, J. C. Y.; Wan, R. C. Y.; Wong, K. Y.; Mhaisalkar, S.; Sheppard, C. J. R.; Olivo, M. Combinatorial Treatment of Photothermal Therapy Using Gold Nanoshells with Conventional Photo-

dynamic Therapy to Improve Treatment Efficacy: An in Vitro Study. *Lasers Surg. Med.* **2008**, *40*, 584−589.
(14) Hirsch, L. R.; Stafford, R. J.; Bankson, J. A.; Sershen, S. R.; Rivera, B.; Price, R. E.; Hazle, J. D.; Halas, N. J.; West, J. L. Nanoshell-Mediated Near-Infrared Thermal Therapy of Tumors under Magnetic Resonance Guidance. *Proc. Natl. Acad. Sci. U. S. A.* **2003**, *100*, 13549−13554.
(15) Huang, X. H.; Jain, P. K.; El-Sayed, I. H.; El-Sayed, M. A. Determination of the Minimum Temperature Required for Selective Photothermal Destruction of Cancer Cells with the Use of Immunotargeted Gold Nanoparticles. *Photochem. Photobiol.* **2006**, *82*, 412−417.
(16) Krpetic, Z.; Nativo, P.; See, V.; Prior, I. A.; Brust, M.; Volk, M. Inflicting Controlled Nonthermal Damage to Subcellular Structures by Laser-Activated Gold Nanoparticles. *Nano Lett.* **2010**, *10*, 4549−4554.
(17) Vankayala, R.; Huang, Y.-K.; Kalluru, P.; Chiang, C.-S.; Hwang, K. C. First Demonstration of Gold Nanorods-Mediated Photodynamic Therapeutic Destruction of Tumors via Near Infra-Red Light Activation. *Small* **2014**, *10*, 1612−1622.
(18) Zhao, T.; Shen, X.; Li, L.; Guan, Z.; Gao, N.; Yuan, P.; Yao, S. Q.; Xu, Q.-H.; Xu, G. Q. Gold Nanorods as Dual Photo-Sensitizing and Imaging Agents for Two-Photon Photodynamic Therapy. *Nanoscale* **2012**, *4*, 7712−7719.
(19) Vankayala, R.; Sagadevan, A.; Vijayaraghavan, P.; Kuo, C.-L.; Hwang, K. C. Metal Nanoparticles Sensitize the Formation of Singlet Oxygen. *Angew. Chem., Int. Ed.* **2011**, *50*, 10640−10644.
(20) Vankayala, R.; Kuo, C.-L.; Sagadevan, A.; Chen, P.-H.; Chiang, C.-S.; Hwang, K. C. Morphology Dependent Photosensitization and Formation of Singlet Oxygen ($^1\Delta_g$) by Gold and Silver Nanoparticles and Its Application in Cancer Treatment. *J. Mater. Chem. B* **2013**, *1*, 4379−4387.
(21) Zhang, W.; Li, Y.; Niu, J.; Chen, Y. Photogeneration of Reactive Oxygen Species on Uncoated Silver, Gold, Nickel, and Silicon Nanoparticles and Their Antibacterial Effect. *Langmuir* **2013**, *29*, 4647−4651.
(22) Dougherty, T. J.; Gomer, C. J.; Henderson, B. W.; Jori, G.; Kessel, D.; Korbelik, M.; Moan, J.; Peng, Q. Photodynamic Therapy. *J. Natl. Cancer Inst.* **1998**, *90*, 889−905.
(23) DeRosa, M. C.; Crutchley, R. J. Photosensitized Singlet Oxygen and Its Applications. *Coord. Chem. Rev.* **2002**, *233*, 351−371.
(24) Pasparakis, G. Light-Induced Generation of Singlet Oxygen by Naked Gold Nanoparticles and Its Implications to Cancer Cell Phototherapy. *Small* **2013**, *9*, 4130−4134.
(25) Link, S.; El-Sayed, M. A. Shape and Size Dependence of Radiative, Non-Radiative and Photothermal Properties of Gold Nanocrystals. *Int. Rev. Phys. Chem.* **2000**, *19*, 409−453.
(26) Hartland, G. V. Optical Studies of Dynamics in Noble Metal Nanostructures. *Chem. Rev.* **2011**, *111*, 3858−3887.
(27) Link, S.; El-Sayed, M. A. Optical Properties and Ultrafast Dynamics of Metallic Nanocrystals. *Annu. Rev. Phys. Chem.* **2003**, *54*, 331−366.
(28) Frens, G. Controlled Nucleation for Regulation of Particle-Size in Monodisperse Gold Suspensions. *Nature (London), Phys. Sci.* **1973**, *241*, 20−22.
(29) Turkevich, J.; Stevenson, P. C.; Hillier, J. A Study of the Nucleation and Growth Processes in the Synthesis of Colloidal Gold. *Discuss. Faraday Soc.* **1951**, *11*, 55−75.
(30) Bastus, N. G.; Comenge, J.; Puntes, V. Kinetically Controlled Seeded Growth Synthesis of Citrate-Stabilized Gold Nanoparticles of up to 200 nm: Size Focusing Versus Ostwald Ripening. *Langmuir* **2011**, *27*, 11098−11105.
(31) Dickerson, E. B.; Dreaden, E. C.; Huang, X. H.; El-Sayed, I. H.; Chu, H. H.; Pushpanketh, S.; McDonald, J. F.; El-Sayed, M. A. Gold Nanorod Assisted Near-Infrared Plasmonic Photothermal Therapy (PPTT) of Squamous Cell Carcinoma in Mice. *Cancer Lett.* **2008**, *269*, 57−66.
(32) Merkel, P. B.; Kearns, D. R. Radiationless Decay of Singlet Molecular Oxygen in Solution. An Experimental and Theoretical Study of Electronic-to-Vibrational Energy Transfer. *J. Am. Chem. Soc.* **1972**, *94*, 7244−7253.
(33) Matheson, I. B. C.; Lee, J.; Yamanashi, B. S.; Wolbarsht, M. L. Measurement of Absolute Rate Constants for Singlet Molecular Oxygen ($^1\Delta_g$) Reaction with 1,3-Diphenylisobenzofuran and Physical Quenching by Ground-State Molecular-Oxygen. *J. Am. Chem. Soc.* **1974**, *96*, 3343−3348.
(34) Gomes, A.; Fernandes, E.; Lima, J. L. F. C. Fluorescence Probes Used for Detection of Reactive Oxygen Species. *J. Biochem. Biophys. Methods* **2005**, *65*, 45−80.
(35) Spiller, W.; Kliesch, H.; Wohrle, D.; Hackbarth, S.; Roder, B.; Schnurpfeil, G. Singlet Oxygen Quantum Yields of Different Photosensitizers in Polar Solvents and Micellar Solutions. *J. Porphyrins Phthalocyanines* **1998**, *2*, 145−158.
(36) Zhang, X.-F.; Li, X. The Photostability and Fluorescence Properties of Diphenylisobenzofuran. *J. Lumin.* **2011**, *131*, 2263−2266.
(37) Fujii, M.; Usui, M.; Hayashi, S.; Gross, E.; Kovalev, D.; Kunzner, N.; Diener, J.; Timoshenko, V. Y. Chemical Reaction Mediated by Excited States of Si Nanocrystals - Singlet Oxygen Formation in Solution. *J. Appl. Phys.* **2004**, *95*, 3689−3693.
(38) Singh, A.; McIntyre, N. R.; Koroll, G. W. Photo-Chemical Formation of Metastable Species from 1,3-Diphenylisobenzofuran. *Photochem. Photobiol.* **1978**, *28*, 595−601.
(39) Han, P.; Bartels, D. M. Temperature Dependence of Oxygen Diffusion in H_2O and D_2O. *J. Phys. Chem.* **1996**, *100*, 5597−5602.
(40) Jain, P. K.; Qian, W.; El-Sayed, M. A. Ultrafast Cooling of Photoexcited Electrons in Gold Nanoparticle-Thiolated DNA Conjugates Involves the Dissociation of the Gold-Thiol Bond. *J. Am. Chem. Soc.* **2006**, *128*, 2426−2433.
(41) Hu, M.; Hartland, G. V. Heat Dissipation for Au Particles in Aqueous Solution: Relaxation Time versus Size. *J. Phys. Chem. B* **2002**, *106*, 7029−7033.
(42) Link, S.; El-Sayed, M. A. Spectral Properties and Relaxation Dynamics of Surface Plasmon Electronic Oscillations in Gold and Silver Nanodots and Nanorods. *J. Phys. Chem. B* **1999**, *103*, 8410−8426.
(43) Hodak, J. H.; Henglein, A.; Hartland, G. V. Photophysics of Nanometer Sized Metal Particles: Electron-Phonon Coupling and Coherent Excitation of Breathing Vibrational Modes. *J. Phys. Chem. B* **2000**, *104*, 9954−9965.
(44) Takami, A.; Kurita, H.; Koda, S. Laser-Induced Size Reduction of Noble Metal Particles. *J. Phys. Chem. B* **1999**, *103*, 1226−1232.
(45) Kotaidis, V.; Dahmen, C.; von Plessen, G.; Springer, F.; Plech, A. Excitation of Nanoscale Vapor Bubbles at the Surface of Gold Nanoparticles in Water. *J. Chem. Phys.* **2006**, *124*, 184702.
(46) Siems, A.; Weber, S. A. L.; Boneberg, J.; Plech, A. Thermodynamics of Nanosecond Nanobubble Formation at Laser-Excited Metal Nanoparticles. *New J. Phys.* **2011**, *13*, 043018.
(47) Kovalev, D.; Fujii, M. Silicon Nanocrystals: Photosensitizers for Oxygen Molecules. *Adv. Mater.* **2005**, *17*, 2531−2544.
(48) Lin, Z.; Zhigilei, L. V.; Celli, V. Electron Phonon Coupling and Electron Heat Capacity of Metals under Conditions of Strong Electron-Phonon Nonequilibrium. *Phys. Rev. B: Condens. Matter Mater. Phys.* **2008**, *77*, 075133.
(49) Haiss, W.; Thanh, N. T. K.; Aveyard, J.; Fernig, D. G. Determination of Size and Concentration of Gold Nanoparticles from UV-vis Spectra. *Anal. Chem.* **2007**, *79*, 4215−4221.
(50) Hao, E.; Schatz, G. C. Electromagnetic Fields around Silver Nanoparticles and Dimers. *J. Chem. Phys.* **2004**, *120*, 357−366.
(51) Krpetic, Z.; Davidson, A. M.; Volk, M.; Levy, R.; Brust, M.; Cooper, D. L. High-Resolution Sizing of Monolayer-Protected Gold Clusters by Differential Centrifugal Sedimentation. *ACS Nano* **2013**, *7*, 8881−8890.
(52) Fang, J.; Nakamura, H.; Maeda, H. The EPR Effect: Unique Features of Tumor Blood Vessels for Drug Delivery, Factors Involved, and Limitations and Augmentation of the Effect. *Adv. Drug Delivery Rev.* **2011**, *63*, 136−151.
(53) Jain, S.; Hirst, D. G.; O'Sullivan, J. M. Gold Nanoparticles as Novel Agents for Cancer Therapy. *Br. J. Radiol.* **2012**, *85*, 101−113.

DOI: 10.1021/acs.jpcc.6b02005
J. Phys. Chem. C 2016, 120, 10647−10657

(54) Perez-Hernandez, M.; del Pino, P.; Mitchell, S. G.; Moros, M.; Stepien, G.; Pelaz, B.; Parak, W. J.; Galvez, E. M.; Pardo, J.; de la Fuente, J. M. Dissecting the Molecular Mechanism of Apoptosis During Photothermal Therapy Using Gold Nanoprisms. *ACS Nano* **2015**, *9*, 52−61.
(55) Chen, J.; Glaus, C.; Laforest, R.; Zhang, Q.; Yang, M.; Gidding, M.; Welch, M. J.; Xia, Y. Gold Nanocages as Photothermal Transducers for Cancer Treatment. *Small* **2010**, *6*, 811−817.
(56) von Maltzahn, G.; Park, J.-H.; Agrawal, A.; Bandaru, N. K.; Das, S. K.; Sailor, M. J.; Bhatia, S. N. Computationally Guided Photothermal Tumor Therapy Using Long-Circulating Gold Nanorod Antennas. *Cancer Res.* **2009**, *69*, 3892−3900.
(57) Wang, B.; Wang, J.-H.; Liu, Q.; Huang, H.; Chen, M.; Li, K.; Li, C.; Yu, X.-F.; Chu, P. K. Rose-Bengal-Conjugated Gold Nanorods for *in Vivo* Photodynamic and Photothermal Oral Cancer Therapies. *Biomaterials* **2014**, *35*, 1954−1966.
(58) Khaing Oo, M. K.; Yang, Y.; Hu, Y.; Gomez, M.; Du, H.; Wang, H. Gold Nanoparticle-Enhanced and Size-Dependent Generation of Reactive Oxygen Species from Protoporphyrin IX. *ACS Nano* **2012**, *6*, 1939−1947.
(59) Yang, Y.; Hu, Y.; Du, H.; Wang, H. Intracellular Gold Nanoparticle Aggregation and Their Potential Applications in Photodynamic Therapy. *Chem. Commun.* **2014**, *50*, 7287−7290.
(60) Zhao, T.; Yu, K.; Li, L.; Zhang, T.; Guan, Z.; Gao, N.; Yuan, P.; Li, S.; Yao, S. Q.; Xu, Q.-H.; et al. Gold Nanorod Enhanced Two-Photon Excitation Fluorescence of Photosensitizers for Two-Photon Imaging and Photodynamic Therapy. *ACS Appl. Mater. Interfaces* **2014**, *6*, 2700−2708.
(61) Li, Y.; Wen, T.; Zhao, R.; Liu, X.; Ji, T.; Wang, H.; Shi, X.; Shi, J.; Wei, J.; Zhao, Y.; et al. Localized Electric Field of Plasmonic Nanoplatform Enhanced Photodynamic Tumor Therapy. *ACS Nano* **2014**, *8*, 11529−11542.
(62) Yang, Y.; Gao, N.; Hu, Y.; Jia, C.; Chou, T.; Du, H.; Wang, H. Gold Nanoparticle-Enhanced Photodynamic Therapy: Effects of Surface Charge and Mitochondrial Targeting. *Ther. Delivery* **2015**, *6*, 307−321.
(63) Jiang, C.; Zhao, T.; Yuan, P.; Gao, N.; Pan, Y.; Guan, Z.; Zhou, N.; Xu, Q.-H. Two-Photon Induced Photoluminescence and Singlet Oxygen Generation from Aggregated Gold Nanoparticles. *ACS Appl. Mater. Interfaces* **2013**, *5*, 4972−4977.
(64) Baier, J.; Fuß, T.; Pöllmann, C.; Wiesmann, C.; Pindl, K.; Engl, R.; Baumer, D.; Maier, M.; Landthaler, M.; Bäumler, W. Theoretical and Experimental Analysis of the Luminescence Signal of Singlet Oxygen for Different Photosensitizers. *J. Photochem. Photobiol., B* **2007**, *87*, 163−173.
(65) Tsai, D.-H.; DelRio, F. W.; Keene, A. M.; Tyner, K. M.; MacCuspie, R. I.; Cho, T. J.; Zachariah, M. R.; Hackley, V. A. Adsorption and Conformation of Serum Albumin Protein on Gold Nanoparticles Investigated Using Dimensional Measurements and in Situ Spectroscopic Methods. *Langmuir* **2011**, *27*, 2464−2477.
(66) Chadwick, S. J. Photodynamic and Photothermal Human Cancer Cell Killing Using Gold Nanoparticles. Ph.D. Thesis, University of Liverpool, 2015.

DOI: 10.1021/acs.jpcc.6b02005
J. Phys. Chem. C 2016, 120, 10647−10657